Nicholas Novack,[1] Robert L. Cryderman,[1]
and Trace A. Rimroth[2]

Design and Validation of a Modular Rolling Contact Fatigue/ Rolling-Sliding Contact Fatigue Testing Machine

Citation

N. Novack, R. L. Cryderman, and T. A. Rimroth, "Design and Validation of a Modular Rolling Contact Fatigue/Rolling-Sliding Contact Fatigue Testing Machine," in *Bearing Steel Technologies: 12th Volume, Progress in Bearing Steel Metallurgical Testing and Quality Assurance*, ed. J. M. Beswick (West Conshohocken, PA: ASTM International, 2020), 82–102. http://doi.org/10.1520/STP162320190061[3]

ABSTRACT

A variety of testing machines have been developed to test rolling contact fatigue (RCF) and rolling–sliding contact fatigue (RSCF). Many of the RSCF machines have been designed to run at a fixed slide ratio using a geared driveline between the test specimen and the load wheel, which limits the versatility. As more complex stress states are being studied for applications in bearings and gears, the need has arisen for a modular testing machine that could allow the operator to vary both the Hertzian contact stress and the slide ratio to evaluate the effects of contact conditions and microstructure on RSCF. The solution was to build a machine that applies the contact load with a hydraulic cylinder and varies the slide ratio by driving the specimen and load roller through two independent motors, all of which the operator can control through a customizable LabVIEW interface. The equipment was designed

around a specimen with a 25.4-mm diameter and a 152.4-mm length. This geometry is large enough to allow evaluation of commercial heat treatments and materials; additionally, it is capable of running two wear tracks on each specimen to reduce the number of specimens required. The hydraulic load application system is capable of developing Hertzian contact stress levels up to 3.2 GPa, with higher stresses possible by altering the load wheel geometry (e.g., crown radius). Damage in the test specimens is characterized postmortem through a variety of techniques. Some preliminary test results are presented to demonstrate the capabilities of the test equipment to evaluate the effects of steel microstructure on RSCF.

Introduction

Contact fatigue has long been the primary failure mode in rolling bearings, and it has recently received more attention as the primary failure mode in gears, occurring as a precursor to failure by bending fatigue.[1] As two surfaces are pressed together, a Hertzian stress distribution develops in the subsurface of each part. Cyclic loading results in the propagation of microcracks until they reach the free surface, resulting in material removal known as pitting and spalling.[2] Failure under pure rolling conditions, known as rolling contact fatigue (RCF), has been studied extensively for rolling bearings. Recent research has focused more heavily on rolling–sliding contact fatigue (RSCF), which includes tractive forces from differential surface speeds. This type of loading is very common on gear teeth, which experience contact outside the pitch diameter, resulting in high slide ratios. The addition of a sliding component adds additional shear stresses to both parts, which increases the overall stress state and shifts the peak of the stress distribution closer to the surface, causing accelerated pitting fatigue failure.[1] This manuscript describes the development of a test machine capable of evaluating the effects of steel metallurgical characteristics, surface condition, and lubricants on RSCF under a variety of loading and sliding conditions.

RSCF Machine Considerations

Various machines have been constructed to test contact fatigue. Some machines have been designed to test RCF or RSCF, and some have been designed to test both. RCF testing machines are typically simple because the sample and the load applicators can be driven together. The most notable RCF testing machine is the ball-on-rod design. Because the specimen and load applicators must have different surface speeds, RSCF testing machines are typically more complex, implementing either a gearbox or a second driving mechanism.

BALL-ON-ROD TESTING MACHINES

The ball-on-rod testing machine was developed as a means of reducing cost and time associated with studying materials for bearing applications. The machine uses springs to compress two conical plates onto ball bearings, which press against a rod shaped specimen to create contact pressure. A schematic of this machine as depicted by Glover[3] is shown in **figure 1**. Although this machine is simple and robust, it is only capable of testing RCF.

SINGLE-MOTOR DRIVE

The single-motor RSCF drive design utilizes one motor to turn the two separate shafts. This is typically accomplished by driving one of the shafts and coupling the second shaft to the first through a set of gears. The gearset allows the side-by-side shafts to rotate at different angular velocities.

An example of a single-motor machine as depicted by Kramer and Speer[4] is shown in **figure 2**. Although this design is relatively simple and inexpensive, it puts a number of constraints on the system. With one motor driving two shafts, it is

FIG. 1   Schematic of a ball-on-rod testing machine. Adapted from Glover.[3]
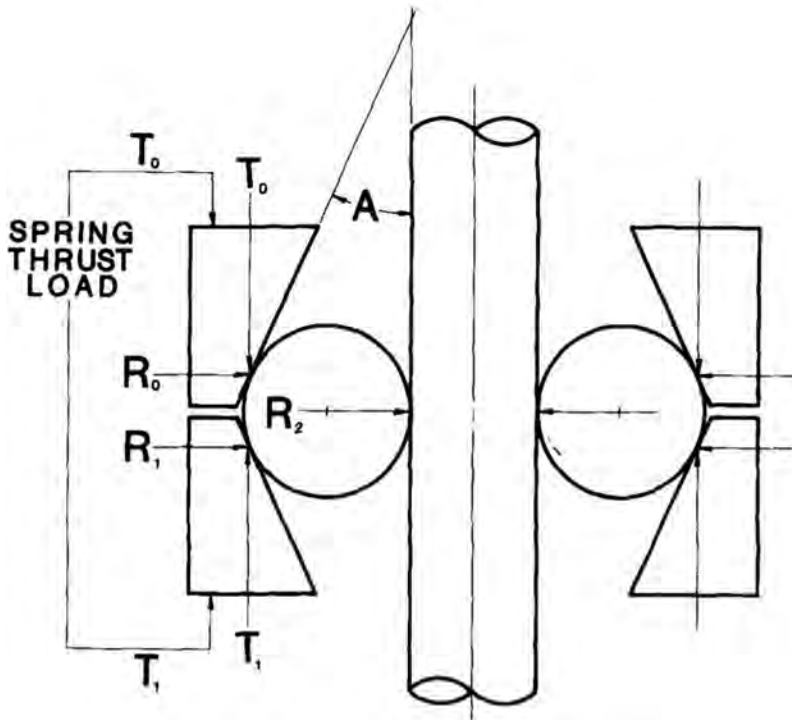
FIG. 2 Schematic of a single-motor driven RSCF machine. Adapted from Kramer and Speer.[4]
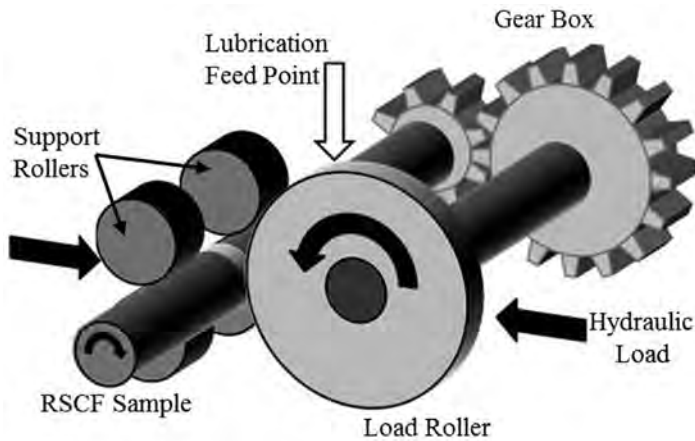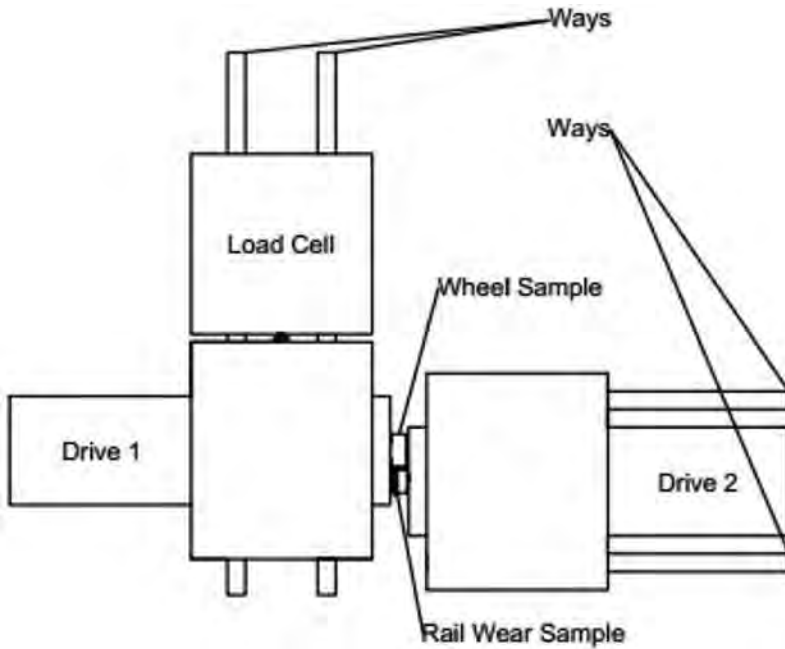

difficult to isolate the torque input on the specimen shaft, which is related to the shear stress being imposed on the surface. Additionally, the gears and drivetrain are subject to backlash, which can affect the instantaneous slide ratio as well as cause excessive vibration. The most notable drawback of the single-motor setup is the lack of modularity in the system. Because the gears must mesh properly, the specimen and load roller diameters must complement the pitch diameters of the gears. Additionally, adjusting the slide ratio requires either a new gearset or a different specimen and load roller geometry, or both.

TWO-MOTOR DRIVE

The two-motor drive design utilizes two motors: one to drive the specimen and one to drive the load roller. Although this design increases the cost and complexity of the test equipment, it allows more control and freedom of test design. Because the specimen and load roller can be driven and controlled independently, their geometries can take precedence and drive the design of the rest of the machine, including motor sizing, driveline design, and platform footprint.

An example of a two-motor drive machine is the Wazau UTM 5000 tribometer, as depicted by Froman and De Moor[5] in figure 3. This machine has two individual driving spindles, each riding on a set of ways that are perpendicular to each other. One of the sets of ways allows the loading, and the other aids in assembly and disassembly. Lubrication is provided by a nozzle above the specimen. This design works very well; however, the specimens are cantilevered out of the spindle, limiting the geometry to machined discs to control the wear track and prevent bending failure at high loads.

Testing Machine Design Goals

The design goals for the testing machine primarily revolved around specimen geometry and versatility, allowing the operator to test materials under a wide variety of parameters. The specimen geometry was to be large enough to accurately simulate industrial heat treatments and components, but small enough to keep material and machining costs reasonable. The drive system was to be designed in such a way to allow independent control of various parameters, including specimen speed, slide ratio, load/contact stress, and lubricant type/temperature. Other goals included designing the system to minimize the effects of misalignment and backlash on the test and, as with all fatigue testing machines, to induce failure in the specimen prior to the machine components.

Overview of Testing Machine

OVERALL ARCHITECTURE

To achieve the goals of the project, the two-motor setup was selected: one motor drives the specimen, while the other drives the load roller. Pressure between the

specimen and load roller is applied by a hydraulic actuator, which is governed by a servo valve working in conjunction with an inline load cell. Lubrication is enabled by a system that pumps oil through a filter to an elevated heating reservoir, gravity-feeds onto the contact point, and drains back into a main reservoir. The machine is controlled through a custom, modifiable program written in LabVIEW.

GEOMETRY

The machine was designed around a 25.4-mm (1-in.) diameter specimen geometry with a length of 152.4 mm (6 in.). The diameter is large enough to accurately conduct industrial heat treatments such as carburizing. The length is short enough to prevent excessive distortion during heat treating, but long enough to accommodate two wear tracks on each specimen, helping to reduce material and machining costs. The specimens are machined out of bars in a manner that avoids the effects of centerline segregation.

The load roller was designed as a disc 127 mm (5 in.) diameter and 12.7 mm (0.5 in.) in width that is carburized 4130 steel. The stress-raising edge effects are eliminated by grinding a crown on the wearing surface. Most testing has been conducted using a 152.4-mm (6-in.) crown radius; however, this geometry can be modified to alter the Hertzian contact stress. Between the larger diameter and the crowned contact surface, the load roller experiences fewer cycles and a lower stress state than the specimen, which ideally allows the specimen to fail first.

The specimen is mounted into a pillow block by a spherical rolling bearing on either side of the wear track. Spherical roller bearings were selected to eliminate any stresses caused by minor misalignment. The distance between the bearings was minimized to prevent specimen bending. Each bearing sits on a tapered sleeve to develop a frictional lock on the specimen. To further prevent axial translation during testing, a set of shaft collars on the specimen sits on either side of the pillow block's oil containment chamber. Thrust bearings between the chamber and the shaft collars allow the specimen to rotate freely. Schematics of the specimen mounted in the pillow block assembly are shown in figure 4.

The load roller is mounted to a 31.8-mm (1.25-in.)-diameter shaft using a keyless locking device. This locking device compresses two tapered sleeves together, expanding the outer diameter and contracting the inner diameter to develop a frictional lock between the shaft and the load roller. The shaft rests on needle roller bearings in a pillow block that opposes that of the specimen. Axial translation is prevented using adjustable shaft collars and thrust bearings that push against either side of the pillow block. The adjustable shaft collars allow the operator to control the axial location of the load roller along the shaft and ensure that it is centered on the specimen wear track. Schematics of the load roller mounted in the pillow block assembly are shown in figure 5. The entire driveline for the load roller sits on a platform that can translate along guide rails by linear slide bearings. This allows the hydraulic force to freely apply load between the load roller and the specimen, and it also allows the operator to separate the pillow blocks for simpler setup and disassembly procedures.

FIG. 4   (*A*) Dimetric and (*B*) cross-section views of the specimen and bearings mounted in the pillow block assembly.
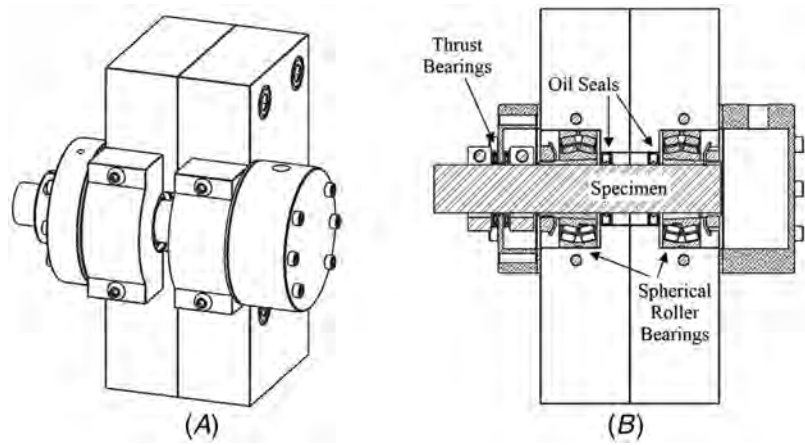
FIG. 5   (*A*) Dimetric and (*B*) cross-section views of the load roller and bearings mounted in the pillow block assembly.
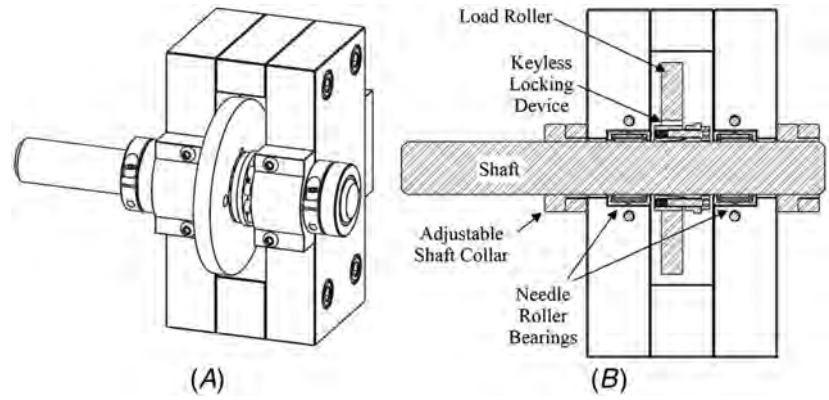
CONTROL INTERFACE

The machine is controlled by a custom LabVIEW program that was designed to allow the operator to monitor the equipment and sensor signals as well as to easily change the operating parameters. The front panel is separated into various clusters for the different parts of the machine. The specimen and load roller speeds can be independently controlled, allowing simple adjustments to the slide ratio. Operating signals such as voltage and current from both motors are displayed to the operator to ensure

that the system is not overloaded. The applied load is controlled by inputting a set point for the load cell. A proportional-integral-derivative (PID) controller reads the signal from the load cell and adjusts the load accordingly. Lubrication is controlled through a manual switch that turns on the pump, a manual valve to control the flow-rate, and a module in the LabVIEW program that controls the temperature. Finally, a separate cluster keeps track of the intensity of vibration and the number of cycles to automatically shut down the machine once the user-defined vibration level or runout limit has been surpassed. An image of the front panel is shown in **figure 6**.

DRIVE SETUP

Due to its more flexible and versatile design, the two-motor drive setup was selected. The specimen is driven by a Baldor EM3219T 7.5-hp motor. The load roller is driven by a Baldor CEM3313T 10-hp motor mated to a Stober 5.4:1 reducing gearbox. This gear reduction increases the driving torque on the load roller and increases the operating speed of the motor, allowing the internal fan to prevent the unit from overheating. The driving shafts incorporate flex-disc couplings that offer a backlash-free solution to accommodating axial and angular misalignment. Both motors are controlled through independent motor drives that translate signals between the motors and the computer. This allows precise control of the operating speed for each motor and sends signals back to the operator regarding the electrical operating parameters for each motor. Communication with the motor drives occurs at a rate of 20 Hz. The torque on the specimen shaft can be referenced to the specimen motor output and is calibrated using an inline Futek TRS705 torque sensor, which can be used to calculate the shear stress on the specimen surface.

**FIG. 6**   Front panel of the LabVIEW program used to control the machine.

FORCE CONTROL

The contact load is applied by means of a double-acting hydraulic cylinder. A hydraulic power supply provides the system with fluid pressurized to 3,000 psi, routed through accumulators to dampen the pressure waves from the pump. An MTS 254.02 servo valve modulates the pressure to actuate the cylinder, which pushes against actuation arms to apply force between the specimen and the load roller. An inline load cell measures the applied force and sends feedback to the PID controller within the LabVIEW program, which sends a signal to the servo valve to adjust the cylinder's applied load. Communication with the servo valve occurs at a rate of 40 Hz. A schematic showing how the load is applied between the load roller and the specimen is illustrated in figure 7.

OIL LUBRICATION SYSTEM

Lubrication can have a significant effect on the results of a contact fatigue test, so a system was designed that allows operation in a variety of conditions, as illustrated in figure 8. A pump pulls oil from a large, insulated reservoir at the bottom of the machine. The oil flows through a 5-μm filter and up to a small, insulated heating reservoir, which contains two 405-W immersion heaters. The oil then gravity-feeds through an insulated hose to a manually adjustable valve sitting right above the specimen to vary the flowrate. After dripping onto the specimen, the oil is collected in a small oil pan and fed back into the main reservoir. The oil pump is wired through a float switch relay in the heating reservoir to maintain the proper flowrate.

FIG. 7 Schematic illustrating how the load is applied between the load roller and the specimen.
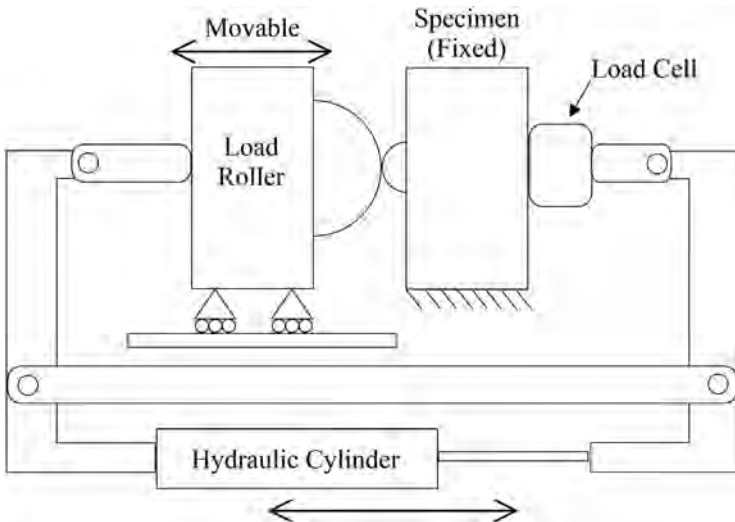
FIG. 8 Schematic of the oil lubrication system, showing (*A*) the Serfilco pump, (*B*) the 5-µm oil filter, (*C*) the elevated heating reservoir, (*D*) the thermocouples, (*E*) the heating elements, (*F*) the float switch, (*G*) the flow control valve, (*H*) the catch pan, and (*I*) the large, insulated reservoir. Adapted from Kramer and Speer.[4]
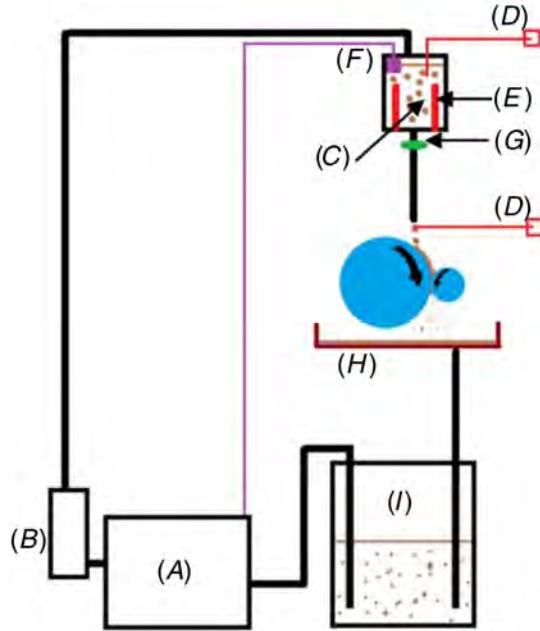

The heaters are controlled by the operator through the LabVIEW program. The operator can select whether or not to heat the oil, and if so, to what temperature. Thermocouples in the heating reservoir and at the nozzle directly above the specimen send feedback to the program, which operates a solid state relay to power on/off the heaters and maintain the proper temperature. Communication with the oil heaters occurs at a rate of 2 Hz. A redundant temperature control system monitors the temperature in the heating reservoir and can cut power to the heaters in the case that an error occurs in the LabVIEW program. The standard lubricant used for testing is Exxon Mobil Jet Oil 254 at 100°C. The maximum achievable temperature depends on several factors, including the type and volume of oil selected.

FAILURE DETECTION

The failure mode of contact fatigue is typically a form of surface loss by means of micropitting, macropitting, or spalling. An accelerometer is magnetically mounted to the specimen bearing block. When a pit forms, significant vibration occurs as the load roller falls in and out of the recession. The LabVIEW program filters the signal from

FIG. 9 Labeled image of the modular RCF/RSCF test machine.
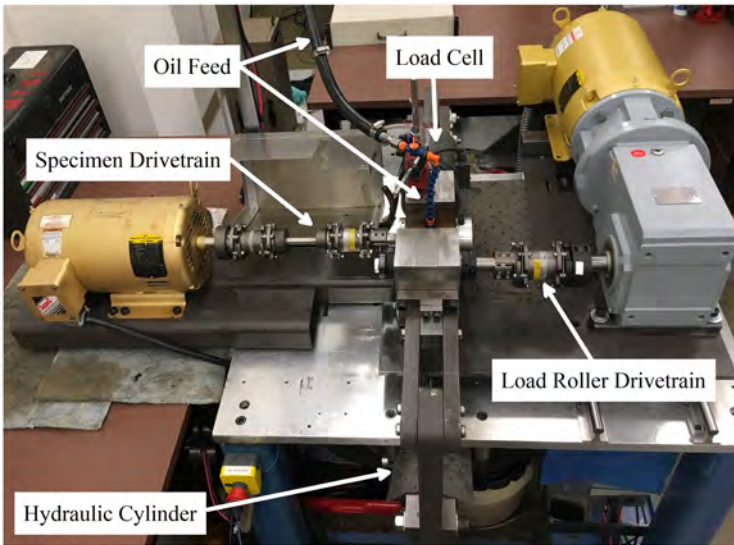
the accelerometer and ends the test when the average vibration climbs significantly above the noise level. Communication with the accelerometer occurs at a rate of 40 Hz.

Machine Overview

A labeled image of the modular RCF/RSCF machine is shown in figure 9. The specimen pillow block assembly and specimen drive motor are bolted to an aluminum baseplate. The load roller motor, gearbox, and pillow block are bolted to a steel plate that is affixed to linear bearings that follow a track affixed to the baseplate. This arrangement allows fine adjustments to ensure all drivetrain components are aligned. The specimen and load roller shafts are aligned independent of the drivetrains. The baseplate sits on a steel frame that contains the hydraulic cylinder, the oil reservoir/pump, and the motor drives. The entire assembly rests on rubber feet to reduce vibrations between the machine and external sources.

Preliminary Testing Results

The machine has been operated to test several samples, most of which fail by pitting prior to ten million cycles. One example is that of a 4320 steel bar of composition noted in table 1. The bar was carburized after machining and grinding. The specimen was tested without further surface preparation after carburizing; this was done to represent the regular operating conditions of commercially carburized parts that are not superfinished after heat treating.

**TABLE 1** Chemical composition (wt.%) of steel grade studied

Alloy	C	Mn	Si	Cr	Ni	Mo	Ti
4320	0.20	0.58	0.28	0.52	1.72	0.22	0.003
Alloy	V	Al	N	S	P	Cu	B
4320	0.005	0.028	0.0100	0.021	0.009	0.21	0.0002

Note: C = carbon; Mn = manganese; Si = silicon; Cr = chromium; Ni = nickel; Mo = molybdenum; Ti = titanium;   V = vanadium;   Al = aluminum;   N = nitrogen;   S = sulfur;   P = phosphorus; Cu = copper; B = boron.

PRETESTING CHARACTERIZATION

The carbon and hardness profiles are shown in **figure 10**. The carbon content was measured by Laboratory Equipment Company (LECO) analysis, and the hardness was measured using an automated Vickers hardness indenter. The residual stresses and retained austenite levels were also measured after carburizing using X-ray diffraction and are shown in **figure 11**. Prior to testing, the surface roughness in the vicinity of the wear tracks of both the specimen and load roller were measured using an optical profilometer, the results of which are shown in **table 2** and **table 3**, respectively. The actual specimen surface roughness readings exceeded the standard test plan because the specimen was not ground after carburizing. The target testing parameters for the bar are listed in **table 4**. The contact stress profile for these conditions, calculated by HertzWin 2.8.0 software, was used to calculate the principal

FIG. 10 Test specimen characteristics for the carburized 4320 steel specimen showing (*A*) carbon profile and (*B*) microhardness profile.
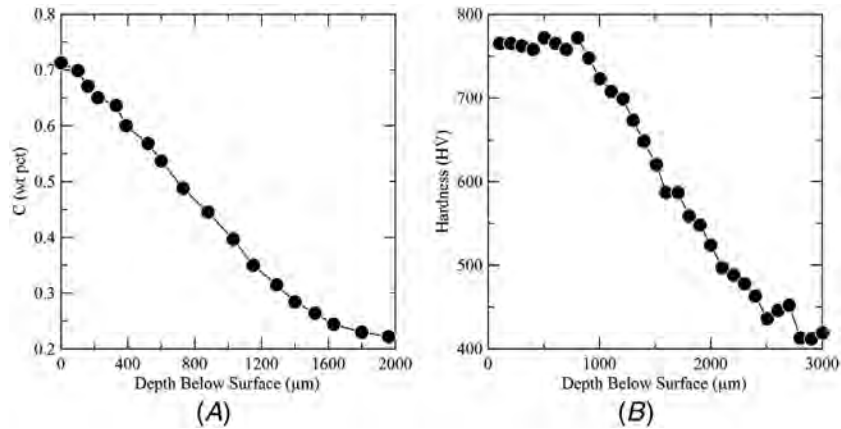
FIG. 11   Test specimen characteristics for the carburized 4320 steel specimen showing
(*A*) residual stress and (*B*) retained austenite profiles.
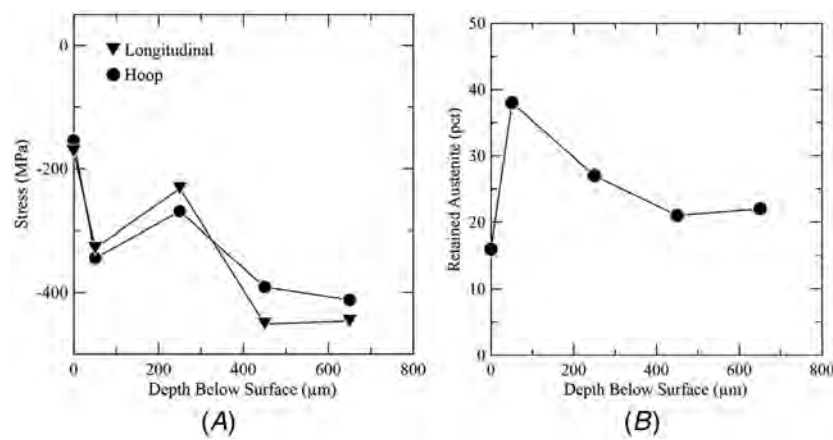
TABLE 2   Initial surface roughness of the specimen

Parameter	Test 1	Test 2	Test 3	Average
Ra, μm	0.75	0.99	0.80	0.85
Rq, μm	1.59	2.18	1.68	1.82
Rz, μm	66.15	76.03	67.22	69.80
Rt, μm	74.82	80.94	75.99	77.25

TABLE 3   Initial surface roughness of the load roller

Parameter	Test 1	Test 2	Test 3	Average
Ra, μm	0.31	0.30	0.34	0.32
Rq, μm	0.38	0.36	0.49	0.41
Rz, μm	8.16	4.57	24.66	12.46
Rt, μm	24.21	6.93	39.94	23.70

stresses, the Von-Mises equivalent stress, and the maximum shear stress, as shown
in figure 12. Under these operating conditions, the specific oil film thickness at the
start of the test was calculated to be 0.033, suggesting that this test was conducted
in the boundary lubrication regime.[6]

TABLE 4   Design test parameters

Test Parameter	Value/Type
Sample Diameter	25.4 mm
Maximum Sample Eccentricity	± 0.0254 mm
Nominal Sample Roughness	0.3–0.4 μm R_a
Specimen Target Case Depth	1.5 mm
Load Roller Material	SAE 4130
Load Roller Diameter	127 mm
Load Roller Crown Radius	152.4 mm
Nominal Load Roller Roughness	0.4 μm R_a
Load Roller Target Case Depth	2 mm
Load Roller Surface Hardness	>700 HV
Hertzian Contact Stress	3.2 GPa
Sample Speed	1,000 RPM
Load Roller Speed	250 RPM
Slide Ratio	−20%
Lubricant Type	Exxon 254 Jet Oil
Lubricant Temperature	100°C
Runout Cycles	10 million

FIG. 12   Contact stress profile calculated by HertzWin 2.8.0 for the given test parameters. The stress state does not include the effects of tractive sliding forces.
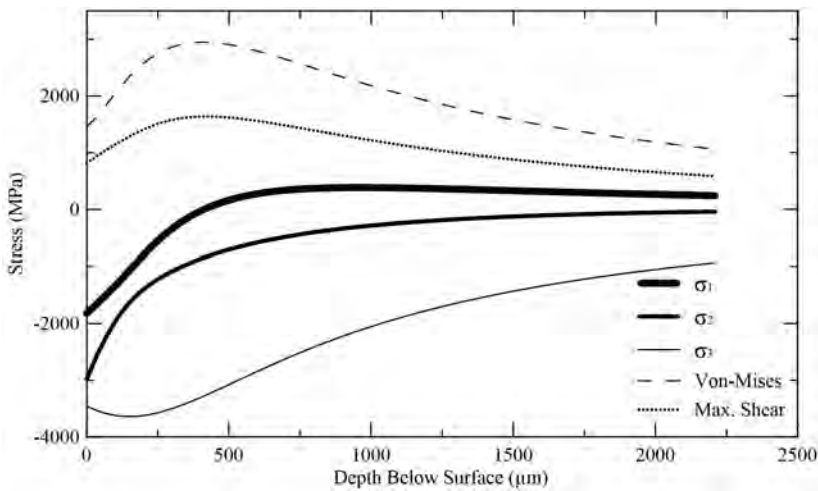
TESTING

Testing begins by loading the specimen into the machine along with a freshly ground load roller disc. After initiating the LabVIEW program, the oil pump and oil heaters are turned on and set to the desired temperature. The motors are turned on and set to a pure rolling condition to prevent uneven heating of the surfaces. Once the target testing temperature is reached, the hydraulic system is powered on with an initial setpoint below zero to prevent the surfaces from contacting. Once the PID controller balances out, the setpoint is increased until the contact load is equal to 75 lbf (81 MPa). The load roller speed is ramped up to achieve the desired slide ratio. Performing this operation at a relatively low load is crucial because it allows the specimen motor to safely reverse its applied torque while maintaining the appropriate output speed. Once the motors have achieved the desired speeds, the contact load is ramped up until the contact pressure reaches 2.5 GPa. This load is held for 5,000 cycles to develop an initial wear track on the specimen. From there, the load is ramped up to the full operating load of 3.2 GPa, at which point the cycle counter begins. Preliminary tests found that ramping up to the 3.2 GPa operating load without developing a wear track required more torque than the 7.5 hp specimen motor could provide. The break-in period allows the surfaces to smooth and reduce the amount of traction at the surface. An illustration of this process is shown in **figure 13**. **Figure 14** shows that the current drawn by the specimen motor

FIG. 13   Specimen motor current plotted as a function of time to illustrate the break-in period. Developing a wear track at 2.5 GPa allows the specimen motor to safely operate below its 20-A limit during the test.
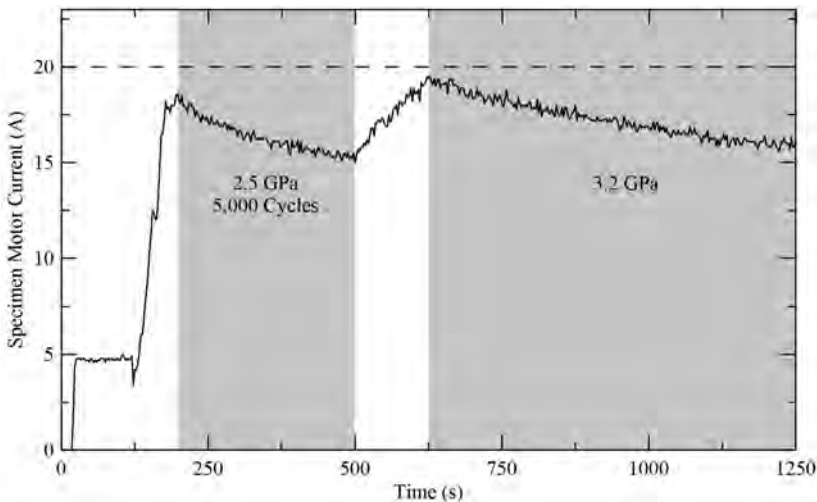
FIG. 14 Current drawn by the specimen motor plotted as a function of cycles, demonstrating how the current draw (torque) approaches a steady-state value after developing a wear track.
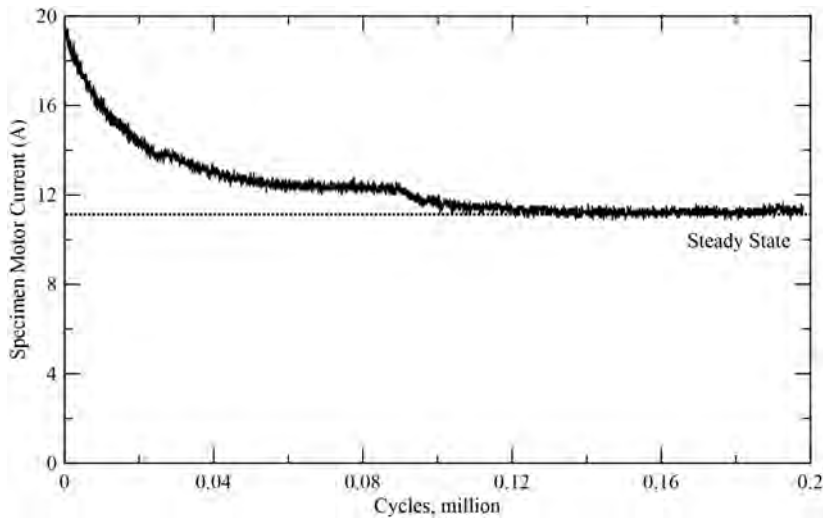

approaches a steady-state value at about 100,000 cycles, indicating completion of wear track development on the specimen.

Once all parameters of the machine have reached their operating setpoints, the machine is nearly autonomous. All systems are controlled through constant communication with the LabVIEW program, which communicates with the machine at various rates and records data at a rate of 0.4 Hz. Evidence of the self-controlling behavior is shown in figure 15, which demonstrates how the PID controller keeps the load within 0.1% of the target. Only occasional supervision is required to ensure that all of the parameters are within their proper operating limits and that the bearings are receiving sufficient lubrication. The machine will automatically stop the test if one of two conditions is met: the cycle counter exceeds the runout limit or the accelerometer detects significant vibration (commonly associated with pitting). Once either of these conditions is met, the contact load is released, the motor speeds are ramped down to zero, the oil heaters are shut down, and an email is sent to the operator.

In the case of the 4320 steel specimen, the accelerometer detected significant vibration and stopped the test after 864,939 cycles. The abrupt spike in vibration is shown in figure 16. Visual observation confirmed that a pit had formed along the wear track. The specimen was unloaded from the machine, cleaned with ethanol, and covered with a greaseless lubricant to protect the surface for further analysis.

FIG. 15   Contact load plotted as a function of cycles, captured at a period midtesting. The average load remains within 0.1% of the target.
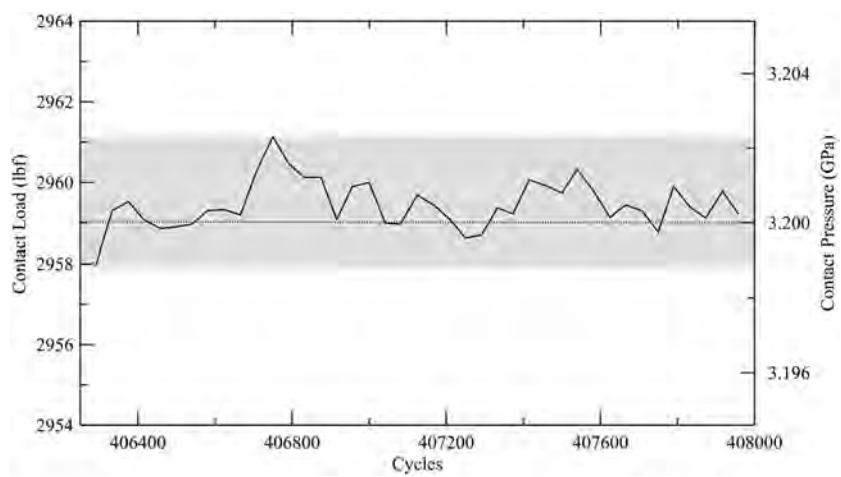
FIG. 16   Vibration plotted as a function of cycles.
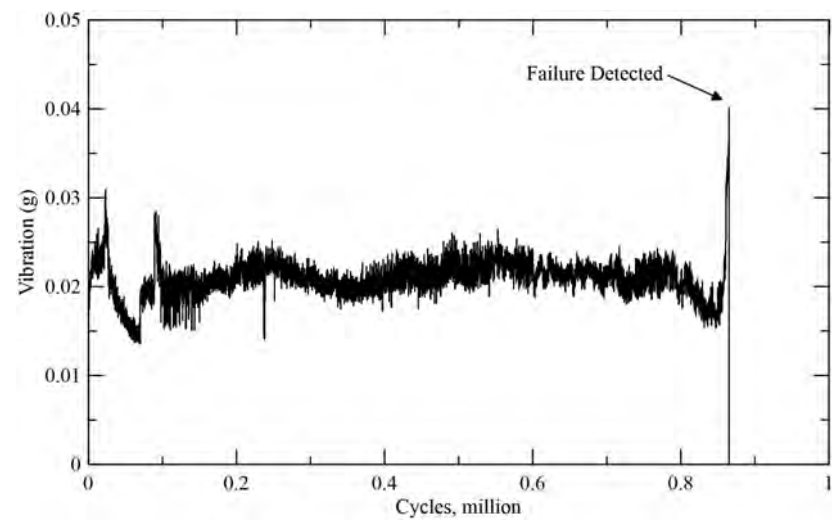
POSTTESTING CHARACTERIZATION

Initial observation of the pit was performed using a Keyence VHX-5000 digital microscope. This machine captures individual images and stitches them together to produce a high-resolution image of the entire pit. For each image, the machine

FIG. 17 Light optical microscope image of the pit that developed along the wear track of the tested 4320 steel bar. The machine used to capture the image was a Keyence VHX-5000. The direction of load movement is up.

translates the lens toward and away from the specimen and selects the most well-focused image for each region, yielding full depth of field. The image that was captured is shown in figure 17.

In addition to light-optical microscopy, the surface roughness along the wear tracks of the specimen and load roller were analyzed and compared to the pretesting values, the results of which are shown in table 5 and table 6. The comparison of

TABLE 5 Surface roughness change along the specimen wear track

Parameter	Pretest Average	Posttest Average	Difference, %
Ra, μm	0.85	0.45	−47.06
Rq, μm	1.82	0.69	−62.09
Rz, μm	69.80	13.10	−80.51
Rt, μm	77.25	18.67	−75.83

TABLE 6 Surface roughness change along the load roller wear track

Parameter	Pretest Average	Posttest Average	Difference, %
Ra, μm	0.32	0.47	+46.88
Rq, μm	0.41	0.58	+41.46
Rz, μm	12.46	6.99	−43.90
Rt, μm	23.70	11.52	−51.39

FIG. 18   Profile along the width of the wear track before and after the test, measured using a Keyence VHX-5000 at 300 × magnification.
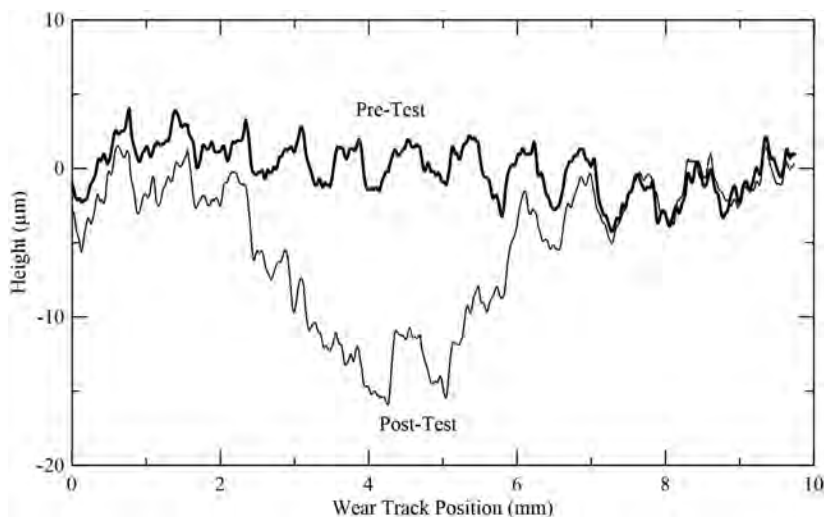

the wear tracks shown in **figure 18** demonstrates the damage that has occurred at the surface, which is attributable to a combination of wear or plastic deformation, or to both.

After imaging and characterizing the pit and the wear track, the specimen is sectioned along the midplane of the wear track for microstructural analysis using the method depicted in **figure 19**. In previous studies by Kramer and Speer,[4] it was found that the additional sliding component altered the orientation and location of the white-etching areas, which are also known as *butterflies* and develop below the surface. While RCF butterflies are typically angled at roughly 45° to the surface, RSCF butterflies were found to develop at much more shallow angles relative to the surface. Additionally, RSCF butterflies were observed in a much broader range of depths than RCF butterflies (0 to 700 µm as opposed to 200 to 400 µm). These differences are believed to be caused by the alteration of stresses imposed by the sliding. A comparison between an RCF butterfly and an RSCF butterfly is shown in **figure 20**.

Summary

Although traditional research focuses on rolling contact fatigue, more attention has recently been drawn to the case of rolling–sliding contact fatigue. A modular testing machine was designed and built to test a wide variety of materials under varying parameters of contact. This flexibility enables the operator to adjust the testing

FIG. 19 Method of sectioning the specimen to analyze the subsurface microstructure after testing. Adapted from Kramer and Speer.[4]
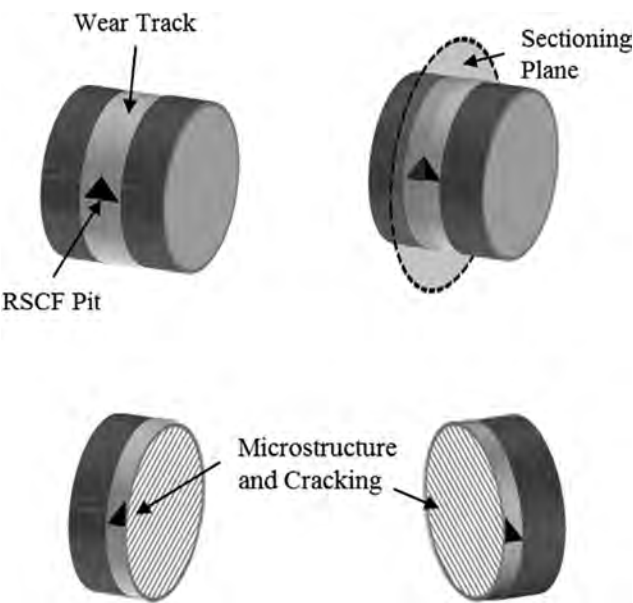
FIG. 20 Comparison of butterflies that formed in the subsurface of gas-carburized 4320 steel bars under (*A*) rolling contact fatigue and (*B*) rolling–sliding contact fatigue. Arrows indicate the direction of motion. Adapted from Kramer.[4]
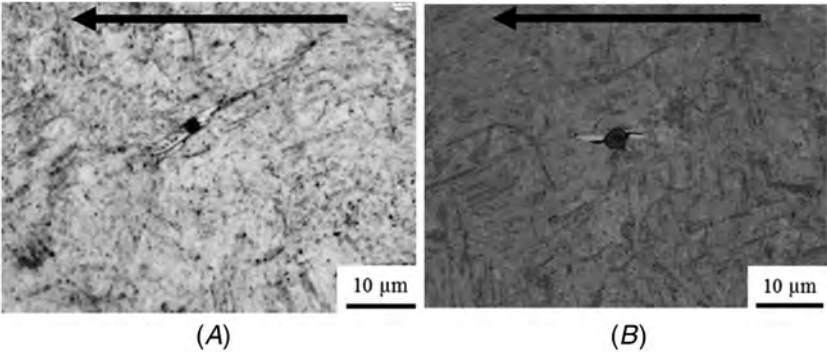
speed, the contact load, the slide ratio, and the lubrication type/temperature with only minor changes to the testing setup. Several tests similar to that which was presented confirm the capability and reliability of the test machine for conducting

Hertzian contact stresses up to 3.2 GPa with a negative slide ratio of 20%. Specimens are characterized before and after testing to observe the damage processes under RSCF and to evaluate the effects of steel microstructure. A test program is underway to investigate the influence of metallurgical features under RSCF conditions.

ACKNOWLEDGMENTS

References

1.   P. J. L. Fernandes and C. McDuling, "Surface Contact Fatigue Failures in Gears," *Engineering Failure Analysis* 4, no. 2 (1997): 99–107, https://doi.org/10.1016/S1350-6307(97)00006-X

2.   R. L. Norton, "Surface Failure," in *Machine Design: An Integrated Approach*, 2nd ed. (Upper Saddle River, NJ: Prentice-Hall, 2000), 443–508.

3.   D. Glover, "A Ball-Rod Rolling Contact Fatigue Tester," in *Rolling Contact Fatigue Testing of Bearing Steels*, ed. J. Hoo (West Conshohocken, PA: ASTM International, 1982), 107–124, https://doi.org/10.1520/STP36135S

4.   P. C. Kramer and J. G. Speer, "An Investigation of Rolling-Sliding Contact Fatigue Damage of Carburized Gear Steels" (master's thesis, Colorado School of Mines, 2014).

5.   J. Froman and E. De Moor, "Effects of Copper on Wear and Rolling-Sliding Contact Fatigue of Rail Steels" (master's thesis, Colorado School of Mines, 2017).

6.   R. L. Norton, "Bearings and Lubrication," in *Machine Design: An Integrated Approach*, 2nd ed. (Upper Saddle River, NJ: Prentice-Hall, 2000), 619–682.